

Impact of Bedding Planes on Mechanical Properties of Sandstone

Shan-chao Hu¹ · Yun-liang Tan¹ · Hui Zhou² · Wei-yao Guo¹ · Da-wei Hu² ·
Fan-zhen Meng^{2,3} · Zhi-gang Liu⁴

Received: 3 November 2016 / Accepted: 17 May 2017 / Published online: 26 May 2017
© Springer-Verlag Wien 2017

Keywords Interbedded sandstone · Compression test · Brazilian disk test · Anisotropy · Fracture mode

1 Introduction

Currently, many underground structures are built in rock masses with bedded structures, such as coal mine roadways (Ning et al. 2017; Tan et al. 2015a, b, 2017), chemical and nuclear waste repositories (Yang et al. 2013) and unconventional oil drilling (Meier et al. 2015). The bedding planes have a considerable influence on the behavior of the rock mass, and it is considered to be critical for slope stability (Ghazvinian et al. 2010). Hence, engineering design and stability analysis of underground structure need to consider the anisotropic properties of bedded rock masses.

The mechanical parameters of bedded rock masses are related to not only the intact rock but also the distribution and properties of the bedding planes. Existing studies have focused on the mechanical properties of bedded rock and carried out conventional compression tests with various loading angles (Niandou et al. 1997; Al-Harathi 1998; Ghazvinian and Hadei 2012; Martínez and Schmitt 2013; Gao et al. 2015; You et al. 2015) to study the deformation, compressive strength and other anisotropic features. In addition, some investigators considered the anisotropic features of the tensile strength of bedded rock and conducted tension tests with various loading angles (e.g., Butenuth et al. 1994; Chen and Hsu 2001; Tavallali and Vervoort 2010a, b; Dan et al. 2013; Ghazvinian et al. 2013).

Based on these research findings, various anisotropic failure criteria and constitutive models have been proposed. A typical one was the single plane of weakness theory proposed by Jaeger (1960). In addition, Duveau and Shao (1998) summarized the previous anisotropic failure criteria in three aspects: mathematical continuous criterion, empirical continuous models and discontinuous weakness plane theories, and he also put forward a modified single-plane-weakness theory (Duveau and Shao 1998). Thereafter, scholars made some extension and development based on the existing failure criteria and constitutive models (e.g., Tien and Kuo 2001; Hu et al. 2013; Asadi and Bagheripour 2015; Mohammad et al. 2015).

Even though the data from compression and tensile tests of rock with different bedding directions are substantial, the failure mechanisms of the rock with different bedding directions subjected to compression and tension remain unclear. To address these problems, laboratory tests were carried out on interbedded sandstone under various loading angles and stress levels, and by means of scanning electron

✉ Yun-liang Tan
yunliangtan@163.com

✉ Hui Zhou
hzhou@whrsm.ac.cn

¹ State Key Laboratory of Mining Disaster Prevention and Control Co-founded by Shandong Province and the Ministry of Science and Technology, Shandong University of Science and Technology, Qingdao 266590, China

² State Key Laboratory of Geomechanics and Geotechnical Engineering, Institute of Rock and Soil Mechanics, Chinese Academy of Sciences, Wuhan 430071, Hubei, China

³ College of Science, Qingdao Technological University, Qingdao 266033, Shandong, China

⁴ Key Laboratory of Deep Coal Resource Mining, Ministry of Education of China, School of Mines, China University of Mining and Technology, Xuzhou 221116, China

microscopy (SEM), the influence of bedding direction and stress level on the failure mechanisms of the rock subjected to compression and tension was conducted. The testing results provide data that can be used for failure criteria and mechanical models of interbedded sandstone.

2 Description of Interbedded Sandstone

The rock studied here is the interbedded sandstone taken from the site of the Ji'ning III coal mine in central Shandong area, China. Due to the sedimentary nature of the geological formation, there are approximately parallel bedding planes that cause anisotropy in the interbedded sandstone, and the value of sandstone RQD was about 47%. The bedding planes were between 0.3 and 2 mm in thickness, and the bedding was mainly composed of carbide, which was dispersed in sandstone matrix in overall appearance. X-ray diffraction was used to identify the

mineral compositions in detail. The average volumetric fractions of different minerals in the rock matrix are as: 47% quartz, 32% feldspars, 10% debris, 6% muscovite and 5% others (zircon and pyrite), and the minerals in bedding planes are as: 39% clay, 32% quartz, 17% debris, 8% pyrite and 4% siderite nodules. The bulk, dry and saturation density are 2.623, 2.591 and 2.655 g/cm³, respectively. The representative porosity is 6.48%, which was calculated from the values of dry and saturation density. In the case of interbedded sandstone, the grain size was not identified in this study, and the average size of quartz and feldspars grains is generally less than 200 μm based on the existing test results (Qiao et al. 2007; Zuo et al. 2010).

3 Experimental Preparation

Two types of laboratory tests were conducted: conventional compression test and indirect tension test. The current study did not consider thermal effects, and all the tests were carried out under the isothermal condition at room temperature (22 ± 2 °C).

3.1 Specimen Preparation

The fragile rock samples were first wrapped with multiple plastic membranes so as to retain their original state. Afterward the rock specimens were processed according to the testing procedures, and only the specimens without any visual damage were selected for the experimental research.

For the convenience of describing the loading angle, a coordinate system was defined (see Fig. 1). The loading angle was defined by the angle θ between the bedding plane and the axial stress σ_1 , which varied from 0° to 90°.

For conventional compression tests, a total of 45 cylindrical specimens (50 mm in diameter and 100 mm in height) were prepared. For indirect tension tests, cylinder specimens with respective diameter and height of 50 and 25 mm were used, and a total of 9 specimens were prepared. The specimen numbers used in the compression and tension tests are shown in Table 1. In comparison with the average size of the quartz and feldspar grains, the size of specimens used was considered as adequate for mechanical testing. Only three bedding angles could be prepared for testing since the interbedded sandstone is very fragile and specimen preparation was difficult. The selected specimens

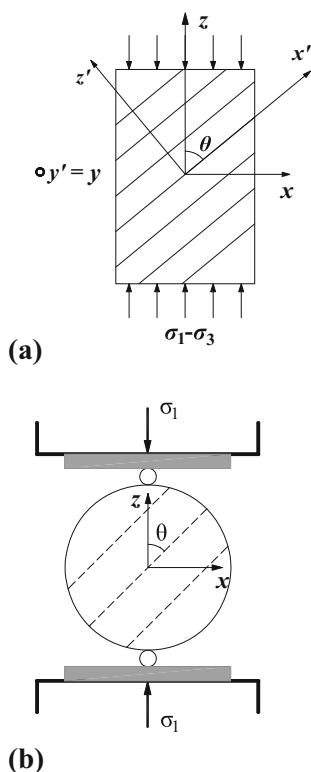


Fig. 1 Definition of loading direction θ . **a** Compression tests, **b** tension test

Table 1 Specimen numbers of compression and tension tests

Testing plan	Confining pressure (MPa)	Loading angle (°)	Total number of specimens	Remarks
Conventional compression tests	0, 5, 10, 20, 30	0, 30, 90	45	3 Specimens per test
Indirect tension tests		0, 45, 90	9	3 Specimens per test

were placed into an incubator so that all specimens were under the condition of identical relative humidity.

3.2 Testing Apparatus and Testing Program

Triaxial and uniaxial compression tests were performed using the MTS 815.03 machine at the Wuhan Institute of Rock and Soil Mechanics (Ren et al. 2016) with a loading rate of 0.001 mm/s (see also Table 1).

Brazilian tests (Zhou et al. 2005; Kazerani et al. 2011; Khanlari et al. 2014; Tan et al. 2015a, b) were performed using the RMT-150c machine (Zhou et al. 2015) with a loading velocity of 0.02 kN/s (see also Table 1).

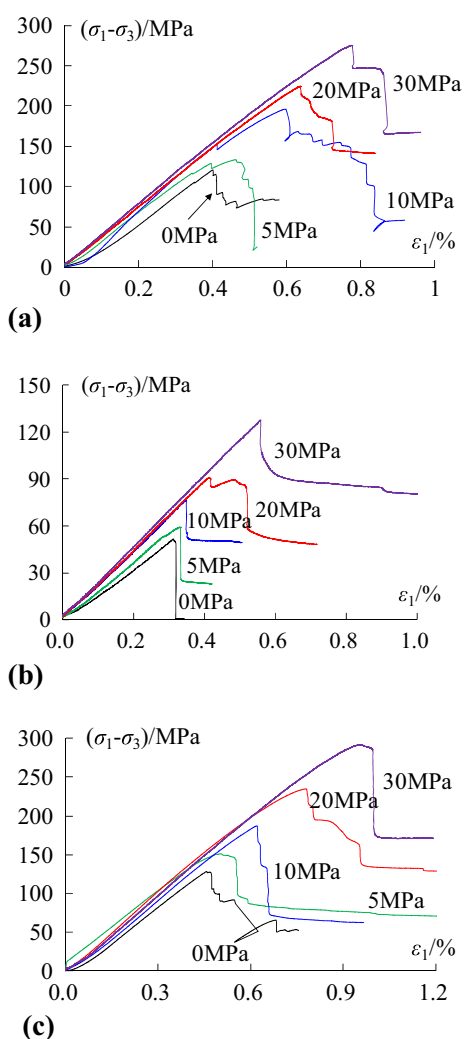


Fig. 2 Typical stress–strain curves during compression tests under different confining pressures (0, 5, 10, 20 and 30 MPa) and for three loading angles (0°, 30° and 90°). **a** Stress–strain curves during compression tests with $\theta = 0^\circ$. **b** Stress–strain curves during compression tests with $\theta = 30^\circ$. **c** Stress–strain curves during compression tests with $\theta = 90^\circ$

4 Conventional Compression Tests

In the compression tests, three specimens were tested for each loading angle and confining pressure, and the average values were used.

4.1 Main Results

In each test, axial and lateral strains were measured as a function of deviatoric stress. Typical stress–strain curves and volumetric strain–axial strain curves under various loading angles and confining pressures are shown in Figs. 2 and 3, respectively. Generally, the mechanical

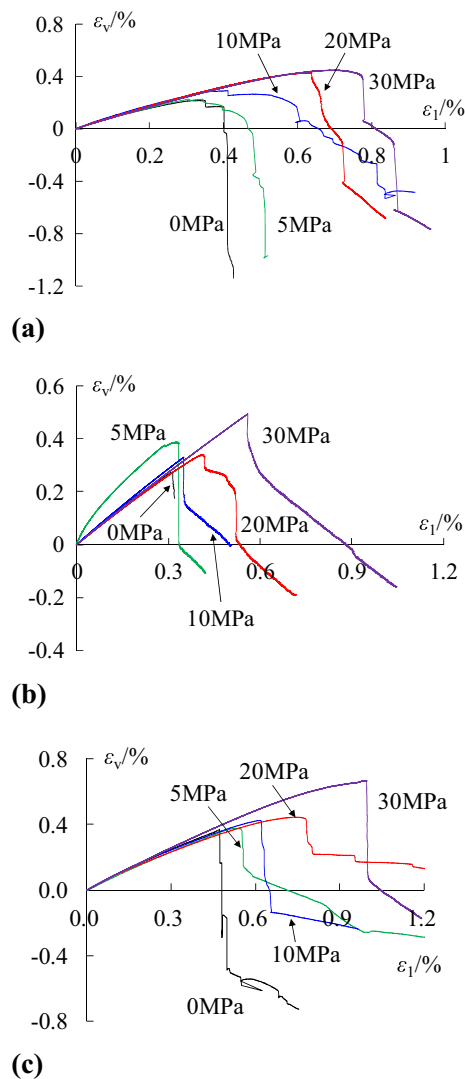


Fig. 3 Typical volumetric strain–axial strain curves during compression tests under different confining pressures (0, 5, 10, 20 and 30 MPa) and for three loading angles (0°, 30° and 90°). **a** Volumetric strain–axial strain curves during compression tests with $\theta = 0^\circ$. **b** Volumetric strain–axial strain curves during compression tests with $\theta = 30^\circ$. **c** Volumetric strain–axial strain curves during compression tests with $\theta = 90^\circ$

characteristics of the interbedded sandstone were significantly impacted by the loading angle and confining pressure, and the obtained results are similar to those obtained by Niandou et al. (1997), Tien et al. (2006), You (2009). Here, we mainly focus on the variation rules of interbedded sandstone deformation, failure features and volumetric compression with the change in loading angles and confining pressures.

- (1) Through comparison of all testing results, the stress–strain curves from various loading angles (Fig. 2) were apparently different, which meant that the interbedded sandstone had apparent anisotropic mechanical behaviors. In addition, under the identical stress state (σ_1 – σ_3 , σ_3), the axial strain at $\theta = 30^\circ$ was apparently larger than that at $\theta = 0^\circ$ and $\theta = 90^\circ$. This indicated that the shear deformation characteristics of bedding planes played an important role in the deformation of the interbedded sandstone.
- (2) The mechanical response of interbedded sandstone exhibited an apparent correlation with the confining pressure. Under a low confining pressure, the specimen was marked by sharp peak stress due to the existing of bedding plane leading to opening (mainly caused by tension failure and sometimes combined shear failure) ($\theta = 0^\circ$, 90°) or sliding failure ($\theta = 30^\circ$) of specimen. Under higher confining pressures, the sharp peak stress state was less pronounced at $\theta = 0^\circ$ and $\theta = 90^\circ$, while the specimen at $\theta = 30^\circ$ still exhibit a clear peak stress. The failure of specimens at $\theta = 0^\circ$ and $\theta = 90^\circ$ was generally associated with the onset of shear or compaction bands (Olsson 1995; Hu et al. 2010; Zhou et al. 2016), and the failure of specimens at $\theta = 30^\circ$ was dominated by the sliding of bedding plane.
- (3) Figure 3a–c indicates that there was a clear transition from volumetric compressibility to dilatancy for almost all confining pressures and loading angles considered. This transition occurred much earlier under a low confining pressure compared with a high confining pressure. At $\theta = 0^\circ$ and $\theta = 90^\circ$, the specimens were first compressed, and then they turned to shear inflation at the inflection point of volumetric strain, but the test at $\theta = 30^\circ$ exhibited a brittle shear inflation at the inflection point of volumetric strain. This was because the volumetric strain resulted in bedding plane transverse extension or compression corresponding to $\theta = 0^\circ$ and $\theta = 90^\circ$, but at the condition of $\theta = 30^\circ$, the specimen exhibited a rapid sliding failure along the bedding plane when the peak value was reached.

4.2 Modulus, Compressive Strength and Compressive Strain at Peak Stress

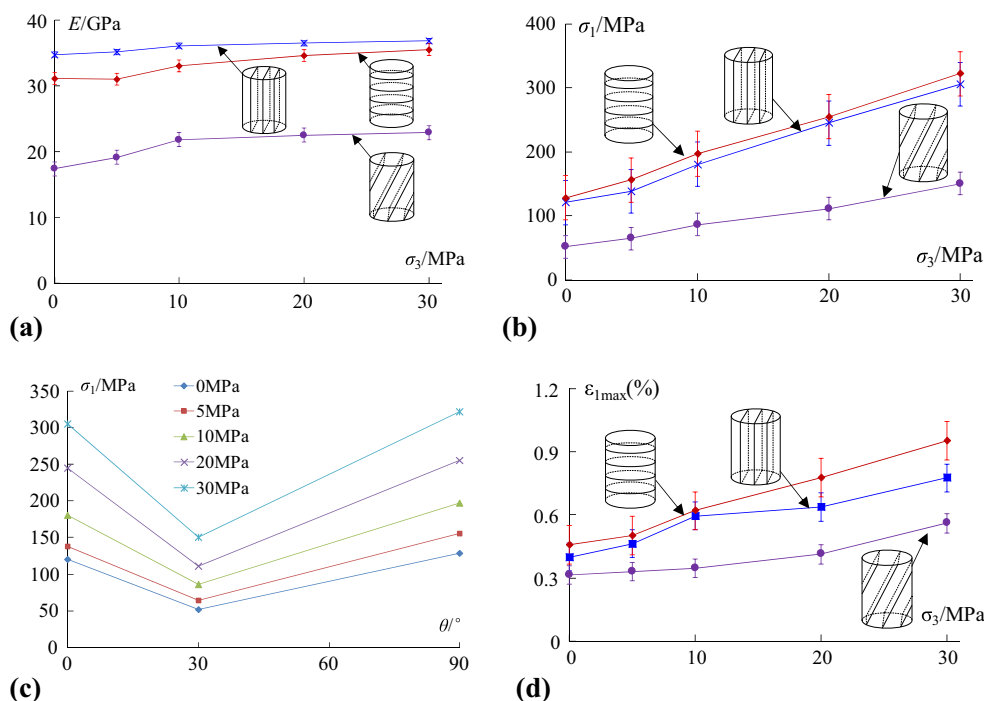
For further analysis, the Young's modulus, peak compressive strength and its corresponding axial strain under various experimental conditions were calculated. The correlation between the corresponding parameters of different loading angles and confining pressures is shown in Fig. 4. The vertical error bars denote the standard error and indicate the range of the parameters over which the data were averaged.

As shown in Fig. 4a, the Young's modulus (E_1) at $\theta = 0^\circ$ was greater than that corresponding to $\theta = 90^\circ$ (E_2). This was because the bedding plane at $\theta = 90^\circ$ closed under the application of axial stress and resulted in a large axial strain, but at $\theta = 0^\circ$, the axial loading was mainly borne by the matrix and therefore, the axial strain was relatively small (Zhao et al. 2017). At $\theta = 30^\circ$, the specimens exhibited a sliding failure along bedding planes, and the corresponding axial strain was apparently larger than the former two; therefore, its Young's modulus was the lowest. The Young's modulus under the three loading angles increased with increasing confining pressure and gradually tended to a fixed value at high confining pressure. The tests on the other types of bedding rock also resulted in similar testing results (Ramamurthy 1993; Nasserri et al. 2003; Zhang et al. 2011).

Figure 4b indicates that the compressive strength of interbedded sandstone is also anisotropic. At loading angles of $\theta = 0^\circ$ and $\theta = 90^\circ$, the compressive strength of sandstone did not differ considerably, and the compressive strength anisotropy (defined as $k_1 = (\sigma_1 - \sigma_3)_0 / (\sigma_1 - \sigma_3)_{90}$) between the two principle structural axes was small. At $\theta = 30^\circ$, its compressive strength was clearly lower than the former two due to different failure modes. To provide indicative values of the failure parameters, we aimed to represent the failure stresses of interbedded sandstone using the Mohr–Coulomb criterion based on the obtained data. The failure parameters of the matrix were determined from failure stresses with $\theta = 90^\circ$ or (and) $\theta = 0^\circ$, while the parameters of the bedding plane were determined based on failure stresses with $\theta = 30^\circ$ (Duveau and Shao 1998). The following values of cohesion and frictional angle were obtained: $c_m = 25.1$ MPa and $\varphi_m = 47^\circ$ for the matrix and $c_b = 14.0$ MPa and $\varphi_b = 32^\circ$ for the bedding plane. It could be easily seen that the failure parameters of the matrix were significantly greater than those of the bedding plane.

Compared with Fig. 4b, the experimental values of compressive strength in the triaxial tests are shown in Fig. 4c as a function of the loading angle. It can be noticed that the compressive strength of the sandstone depended on

Fig. 4 Variation rules of the Young’s modulus, peak strength and the corresponding axial strain under various confining pressures and loading angles (bars donate S.E.). **a** Variation rules of the Young’s modulus of bedding rock under various confining pressures. **b** Variation rules of the failure strength of bedding rock under various confining pressure. **c** Variation rules of the failure strength of bedding rock under various loading angles. **d** Variation rules of axial strain corresponding to the peak strength of bedding rock under various confining pressures



the loading angle θ . For all confining pressures, the compressive strength first decreased and then increased with increasing loading angle from $\theta = 0^\circ$ to 90° . There were two maximum strength values at $\theta = 0^\circ$ and $\theta = 90^\circ$, and minimum strength was found at $\theta = 30^\circ$.

Figure 4d represents the statistical values of the axial strain corresponding to the peak stress values at various loading angles. First, under all confining conditions, the axial strain at the loading angle of $\theta = 90^\circ$ was slightly larger than that at $\theta = 0^\circ$. This was because the bedding plane at $\theta = 90^\circ$ gradually closed under the vertical axial loading, but the deformation of the bedding plane parallel to axial loading at $\theta = 0^\circ$ had little impact on axial deformation. The axial strain at $\theta = 30^\circ$ was the lowest before failure because the rock with such a loading angle failed under a lower compressive strength. Besides, under various loading angles, axial strain increased with increasing confining pressure. This was because the increase in confining pressure improved the bearing capacity of specimens; therefore, the axial strain increased correspondingly when it reached the peak compressive strength value.

There were certain discrepancies among various testing results. This kind of discrepancies was primarily caused by the initial nonuniformity and random bedding occurrence. However, the testing results also revealed the bedding plane of sandstone played a determinant role in its deformation and compressive strength. Even though there were discrepancies for the testing results in a certain range, it did not generally overshadow the transverse

anisotropy features of compressive strength and deformation.

4.3 Verification of Modified Single-Plane-Weakness Theory

Following the previous description of the impact of the bedding plane on the compression mechanisms, we used the presented data to check the validity of one of the widely used failure criterion, i.e., the single-plane-weakness theory, which was proposed by Jaeger (1960). In this theory, the anisotropic material is seen as an isotropic body containing one set of weakness planes. The failure of the rock matrix and weakness planes are both described by the Mohr–Coulomb criterion: $\tau = c_m + \sigma \tan \varphi_m$ for the rock matrix and $\tau_\theta = c_b + \sigma_\theta \tan \varphi_b$ for weakness planes, where τ_θ and σ_θ are the shear and normal stress, respectively, applied to the weakness plane at the orientation θ . The failure parameters of the matrix are different from those of the weakness planes: c_m and φ_m are the respective cohesion and frictional angles of the matrix, and c_b and φ_b are the respective cohesion and frictional angles of the weakness planes.

Using the failure criterion and parameters obtained above, the compressive strength in the triaxial tests was calculated. Taking the results of the confining pressures 5 and 20 MPa as an example, a comparison with the test data and the predictions based on the failure criterion is presented in Fig. 5. The calculation results showed a good agreement with the test results, indicating that the failure

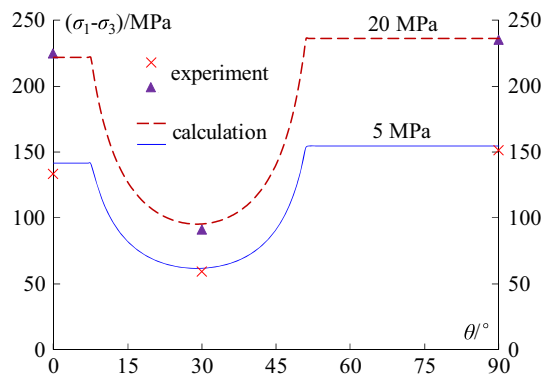


Fig. 5 Comparison between experimental failure stress and calculation data obtained using the Jaeger criterion in the triaxial test performed under different loading angles and confining pressures

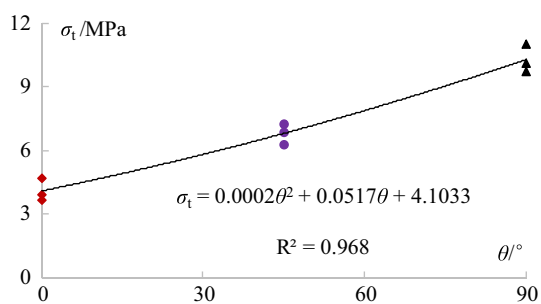


Fig. 6 Correlation between the tensile strength of sandstone and loading angles

criterion could well describe the failure behavior of the stratified rocks.

5 Indirect Tensile Tests

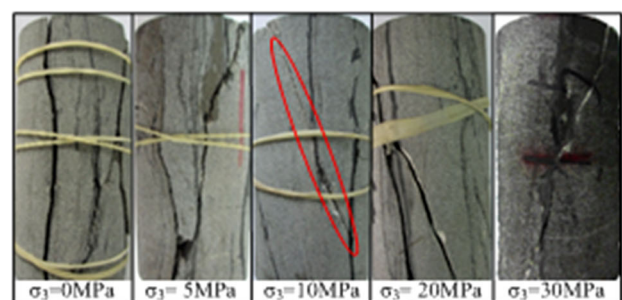
Three specimens were tested for each loading angle in the tension test (Brazilian Test), and the average values were calculated. Figure 6 shows the variation in the tensile strength of the interbedded sandstone with the change in loading angles. The tensile strength of interbedded sandstone was also significantly impacted by the structural anisotropy of the rock. Generally, the tensile strength of the rock specimen increased with increasing loading angles, which was mainly determined by the bearing capacity of the bedded sandstone. At $\theta = 0^\circ$, the specimen exhibited bedding plane activation, and the fractures spread along the bedding plane (Tavallali and Vervoort 2010a, b). When the angle increased to $\theta = 45^\circ$, the fractures cut through the bedding plane, and finally the fractures normal to the isotropic bedding plane became dominant ($\theta = 90^\circ$). As the cohesion of the bedding plane was significantly lower than that of the matrix, the tensile strength increased with increasing loading angles, and this is the base of the following further discussion.

6 Discussion

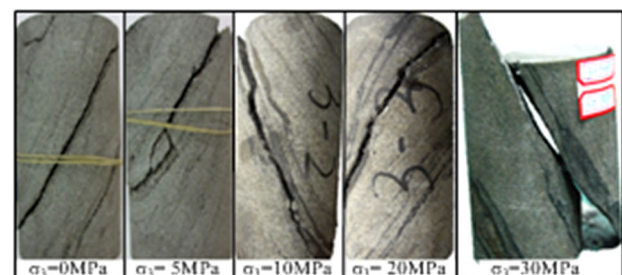
The text above mainly analyzed the macroscopic behavior of interbedded sandstone under various testing conditions. In fact, the macroscopic failure of the rock is closely related to its internal microstructure (Meng et al. 2015). This section discusses the failure mechanisms of interbedded sandstone under various testing conditions by analyzing the fracture modes of the bedding rock using SEM.

6.1 Conventional Compression Tests

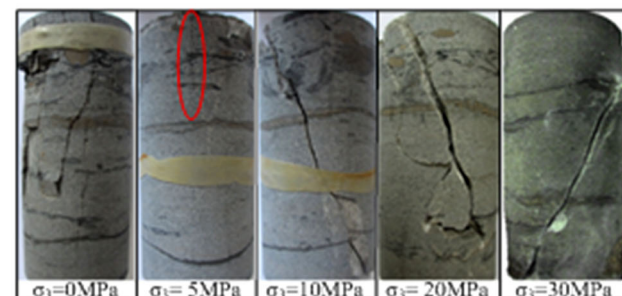
The failure mode of interbedded sandstone under different testing conditions is shown in Fig. 7. At $\theta = 0^\circ$ and $\theta = 90^\circ$, the failure of the specimen evolved from opening under low confining pressure ($\sigma_3 = 0, 5$ MPa) to shear failure under high confining pressure ($\sigma_3 = 10, 20$,



(a)



(b)



(c)

Fig. 7 Failure modes of compression test specimens under various loading angles **a** $\theta = 0^\circ$, **b** $\theta = 30^\circ$ and **c** $\theta = 90^\circ$

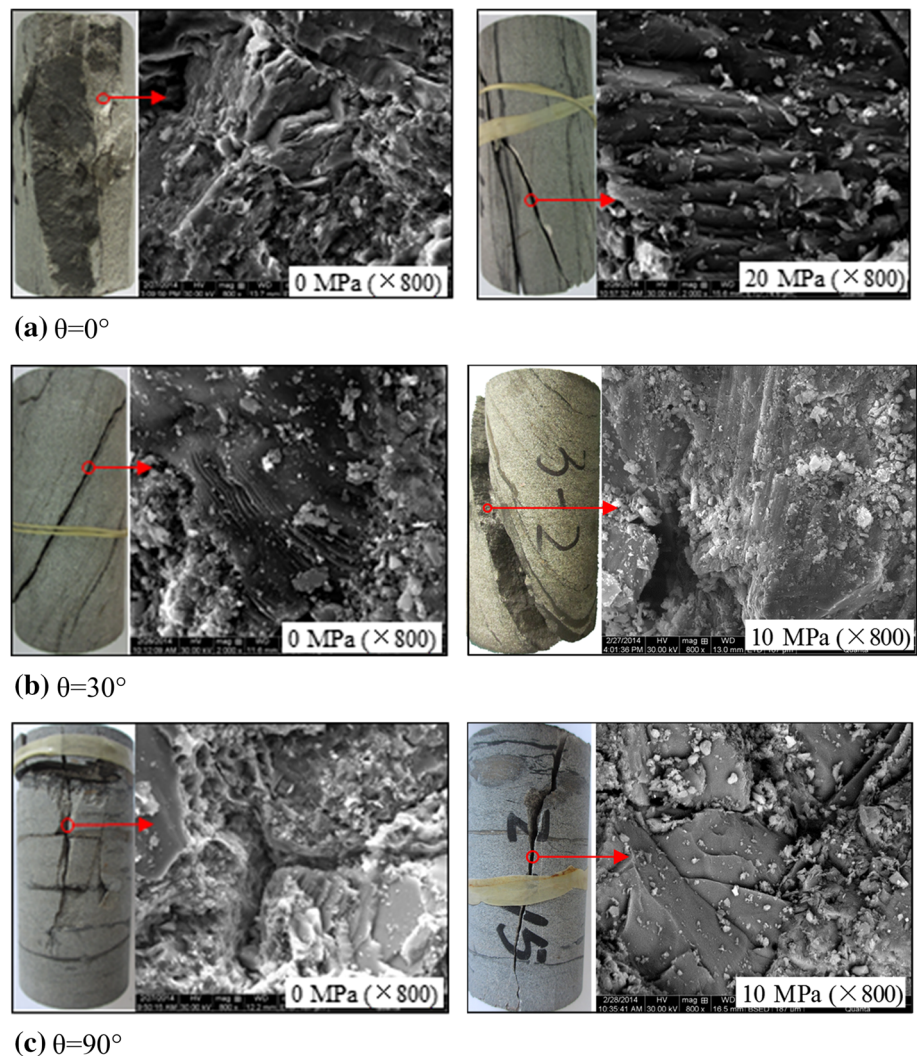
30 MPa); at $\theta = 30^\circ$, the fractures under various confining pressures were all in the bedding plane. Furthermore, the specimens with a typical fracture surface from uniaxial and triaxial compression tests were selected, and the results of the SEM image are shown in Fig. 8. The fracture surfaces of specimens with loading angles of $\theta = 0^\circ$ and $\theta = 90^\circ$ were similar. Under uniaxial compression condition, the edges of the fracture were sharp, and there were few fragments scattered in the lower position. The fracture mode was mostly an intergranular fracture pattern that showed obvious characteristics of tension failure. For the triaxial test, the branches of fractures were approximately parallel and densely spread. The height of steps was smaller than that under tension failure, and the transgranular fracture occurred on the fracture surfaces, representing apparent shear failure. At the loading angle of $\theta = 30^\circ$, the rock failure exhibited clear cleavage steps on its surface and represented an apparent shear failure property. It was thus observed that the different failure modes were the root

cause of the difference in fracture appearance and mechanical properties of the compression failure of the interbedded sandstone.

6.2 Indirect Tensile Tests

Figure 9 shows the failure mode and SEM images from the failed specimen fracture of the tensile tests under various loading angles. A comparison of the results revealed that when the tensile stress was normal to the bedding plane, the fracture morphology exhibited an intergranular fracture pattern along the bedding plane with a small grain-cutting pattern ($\theta = 0^\circ$). When the tensile stress was parallel to the bedding plane ($\theta = 90^\circ$), the bedding plane deformation had little impact on the overall failure, and the failure mode was primarily intergranular fracture of the matrix. At $\theta = 45^\circ$, the fracture mode changed to coupled intergranular fracture and transgranular fracture. It was thus observed that similar to the

Fig. 8 Scanning electron microscopy of compression failure of interbedded sandstone. **a** $\theta = 0^\circ$, **b** $\theta = 30^\circ$ and **c** $\theta = 90^\circ$



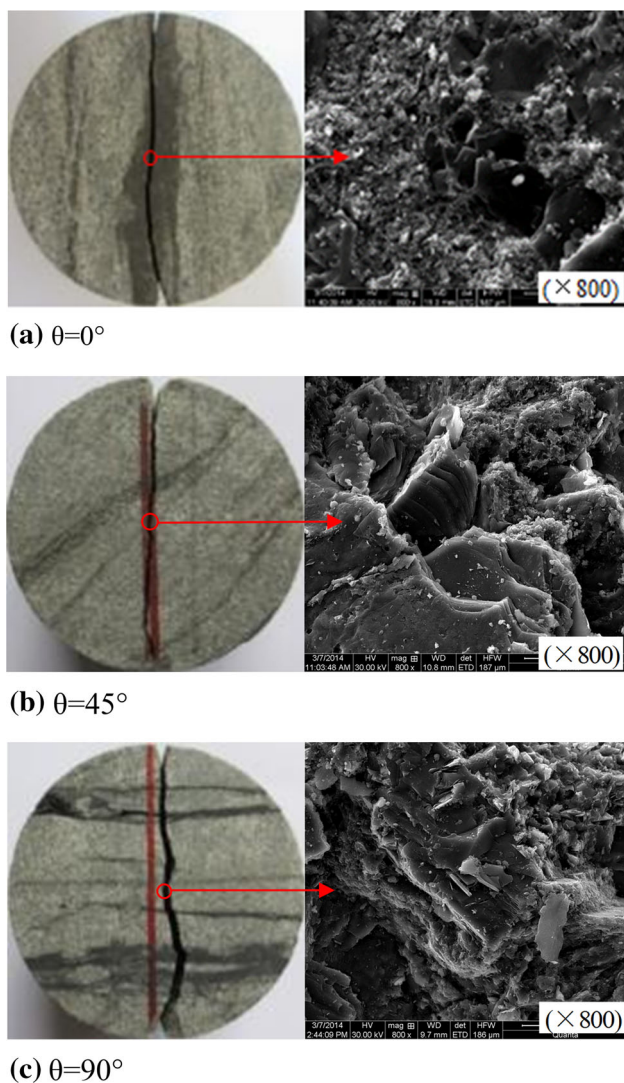


Fig. 9 Scanning electron microscopy of tension failure of interbedded sandstone. **a** $\theta = 0^\circ$, **b** $\theta = 30^\circ$ and **c** $\theta = 90^\circ$

compression tests, the different failure modes were the root cause of the difference in the tensile mechanical properties of the interbedded sandstone.

7 Conclusions

In this study, laboratory compression tests were carried out on the interbedded sandstone under various confining pressures and loading angles as well as tension tests under various loading angles. The testing results revealed that the mechanical properties of the interbedded sandstone were significantly influenced by stress levels and structural anisotropy. The Young's modulus of sandstone at a loading angle of $\theta = 0^\circ$ was greater than that at $\theta = 90^\circ$, and both were apparently greater than that at $\theta = 30^\circ$. The variation rules of sandstone compressive strength with the change on

loading angles were similar to those of the Young's modulus, and all exhibited apparent brittle failure features. The axial strain corresponding to the peak compressive stress at $\theta = 90^\circ$ was greater than that at $\theta = 0^\circ$, and the axial strain at $\theta = 30^\circ$ was relatively small as the peak compressive strength was low. The tensile strength of sandstone increased with increasing the loading angle. This was because the failure of specimens evolved from bedding plane activation to the tensile failure of the matrix. Finally, this research investigated the root causes of the mechanical property variation of the interbedded mechanical properties through electron microscopy scanning of tested specimens with typical failure.

Acknowledgements The research described in this paper was financially supported by the National Natural Science Foundation of China (Nos. 51274133, 51474137, 41172288 and 51609121), National Program on Key Basic Research Project of China under Grant No. 2014CB046902, Tai'shan Scholar Engineering Construction Fund of Shandong Province of China, China Postdoctoral Science Foundation Funded Project (No. 2016M592220), Taishan Scholar Talent Team Support Plan for Advanced and Unique Discipline Areas, and Qingdao Postdoctoral Applied Research Project (No. 2015198). We also thank Professor Baotang Shen and LetPub for the linguistic assistance during the preparation of this manuscript.

References

- Al-Harathi AA (1998) Effect of planar structures on the anisotropy of Ranyah sandstone, Saudi Arabia. *Eng Geol* 50(97):49–57
- Asadi M, Bagheripour MH (2015) Modified criteria for sliding and non-sliding failure of anisotropic jointed rocks. *Int J Rock Mech Min* 73:95–101
- Butenuth C, Freitas MHD, Park HD, Schetelig K, Lent PV, Grill P (1994) Observations on the use of the hoop test for measuring the tensile strength of anisotropic rock. *Int J Rock Mech Geomech Abstr* 31(6):733–741
- Chen CS, Hsu SC (2001) Measurement of indirect tensile strength of anisotropic rocks by the ring test. *Rock Mech Rock Eng* 34(4):293–321
- Dan DQ, Konietzky H, Herbst M (2013) Brazilian tensile strength tests on some anisotropic rocks. *Int J Rock Mech Min* 58:1–7
- Duveau G, Shao JF (1998) A modified single plane of weakness theory for the failure of highly stratified rocks. *Int J Rock Mech Min* 35(6):807–813
- Duveau G, Shao JF, Henry JP (1998) Assessment of some failure criteria for strongly anisotropic geomaterials. *Mech Cohes-Frict Mat* 3(1):1–26
- Gao Q, Tao JL, Hu JY, Yu B (2015) Laboratory study on the mechanical behaviors of an anisotropic shale rock. *J Rock Mech Geotech Eng* 7(2):213–219
- Ghazvinian A, Hadei MR (2012) Effect of discontinuity orientation and confinement on the strength of jointed anisotropic rocks. *Int J Rock Mech Min* 55(10):117–124
- Ghazvinian AH, Taghichian A, Hashemi M, Mar'ashi SA (2010) The shear behavior of bedding planes of weakness between two different rock types with high strength difference. *Rock Mech Rock Eng* 43(1):69–87
- Ghazvinian A, Vaneghi RG, Hadei MR, Azinfar MJ (2013) Shear behavior of inherently anisotropic rocks. *Int J Rock Mech Min* 61(7):96–110

- Hu DW, Zhou H, Zhang F, Shao JF (2010) Evolution of poroelastic properties and permeability in damaged sandstone. *Int J Rock Mech Min* 47(6):962–973
- Hu DW, Zhou H, Zhang F, Shao JF, Zhang JF (2013) Modeling of inherent anisotropic behavior of partially saturated clayey rocks. *Comput Geotech* 48(48):29–40
- Jaeger JC (1960) Shear failure of anisotropic rocks. *Geol Mag* 97(01):65–72
- Kazerani T, Yang ZY, Zhao J (2011) A discrete element model for predicting shear strength and degradation of rock joint by using compressive and tensile test data. *Rock Mech Rock Eng* 45(5):1–15
- Khanlari G, Rafiei B, Abdilor Y (2014) Evaluation of strength anisotropy and failure modes of laminated sandstones. *Arab J Geosci* 8(5):3089–3102
- Martínez JM, Schmitt DR (2013) Anisotropic elastic moduli of carbonates and evaporites from the Weyburn-Midale reservoir and seal rocks. *Geophys Prospect* 61(2):363–379
- Meier T, Rybacki E, Backers T, Dresen G (2015) Influence of bedding angle on borehole stability: a laboratory investigation of transverse isotropic oil shale. *Rock Mech Rock Eng* 48(4):1535–1546
- Meng FZ, Zhou H, Zhang CQ, Xu RC, Lu JJ (2015) Evaluation methodology of brittleness of rock based on post-peak stress-strain curves. *Rock Mech Rock Eng* 48(5):1787–1805
- Mohammad R, Mostafa A, Abbas M, Hossaini MF (2015) Prediction of representative deformation modulus of longwall panel roof rock strata using Mamdani fuzzy system. *Int J Min Sci Tech* 25(1):23–30
- Nasser MHB, Rao KS, Ramamurthy T (2003) Anisotropic strength and deformational behavior of Himalayan schists. *Int J Rock Mech Min* 40(1):3–23
- Niandou H, Shao JF, Henry JP, Fourmaintraux D (1997) Laboratory investigation of the mechanical behaviour of Tournemire shale. *Int J Rock Mech Min* 34(1):3–16
- Ning JG, Wang J, Tan YL, Zhang LS, Bu TT (2017) In situ investigations into mining-induced overburden failures in close multiple-seam longwall mining: a case study. *Geomech Eng* 12(4):657–673
- Olsson W (1995) Development of anisotropy in the incremental shear moduli for rock undergoing inelastic deformation. *Mech Mater* 21:231–242
- Qiao LP, Liu J, Feng XT (2007) Study on damage mechanism of sandstone under hydro-physico-chemical effects. *Chin J Rock Mech Eng* 26(10):2117–2124 (**in Chinese**)
- Ramamurthy T (1993) Strength and modulus response of anisotropic rocks, chap 13. *Comprehensive rock engineering*, vol I. Pergamon Press, Oxford, pp 313–329
- Ren GM, Wu H, Fang Q, Liu JZ, Gong ZM (2016) Triaxial compressive behavior of UHPCC and applications in the projectile impact analyses. *Constr Build Mater* 113:1–14
- Tan X, Konietzky H, Frühwirth T, Dan DQ (2015a) Brazilian tests on transversely isotropic rocks: laboratory testing and numerical simulations. *Rock Mech Rock Eng* 48(4):1341–1351
- Tan YL, Yu FH, Ning JG, Zhao TB (2015b) Design and construction of entry retaining wall along a gob side under hard roof stratum. *Int J Rock Mech Min* 77:115–121
- Tan YL, Liu XS, Ning JG, Lv YW (2017) In situ investigations on failure evolution of overlying strata induced by mining multiple coal seams. *Geotech Test J* 40(2):1–14
- Tavallali A, Vervoort A (2010a) Failure of layered sandstone under Brazilian test conditions: effect of micro-scale parameters on macro-scale behaviour. *Rock Mech Rock Eng* 43(5):641–653
- Tavallali A, Vervoort A (2010b) Effect of layer orientation on the failure of layered sandstone under Brazilian test conditions. *Int J Rock Mech Min* 47(2):313–322
- Tien YM, Kuo MC (2001) A failure criterion for transversely isotropic rocks. *Int J Rock Mech Min* 38(3):399–412
- Tien YM, Kuo MC, Juang CH (2006) An experimental investigation of the failure mechanism of simulated transversely isotropic rocks. *Int J Rock Mech Min* 43(8):1163–1181
- Yang DS, Chanchole S, Valli P, Chen LF (2013) Study of the anisotropic properties of argillite under moisture and mechanical loads. *Rock Mech Rock Eng* 46(2):247–257
- You MQ, Su CD (2009) Study on the deformation, failure and strength of sandstone with various declined bedding. *J Henan Polytech Univ (Nat Sci)* 28(5):626–635 (**in Chinese**)
- You S, Ji HG, Labiouse V, Hall SA, Viggiani G (2015) Quantitative analysis of deformation in hollow cylinder tests on anisotropic clay formations. *Int J Min Sci Tech* 25(2):299–303
- Zhang JC, Peng L, Xu XH, Zhu NW, Fang LG (2011) Experimental study of elastoplastic coupling deformation for transversely isotropic rocks. *Chin J Rock Mech Eng* 30(2):267–274 (**in Chinese**)
- Zhao TB, Fang K, Wang L, Zou JC, Wei MY (2017) Estimation of elastic modulus of rock using modified point-load test. *Geotech Test J* 40(2):329–334
- Zhou YH, Zhou DP, Tao Y, Feng ZJ (2005) Experimental investigation on shear strength parameters of jointed rock mass. *J Southwest Jiaotong Univ* 40(1):73–76 (**in Chinese**)
- Zhou H, Xu RC, Zhang CQ, Shen Z, Meng FZ, Liu HT (2015) Experimental study of crack prevention effect of pre-stressed bolt anchoring. *Chin J Rock Mech Eng* 34(10):2027–2037 (**in Chinese**)
- Zhou H, Hu D, Zhang F, Shao JF, Feng XT (2016) Laboratory investigations of the hydro-mechanical–chemical coupling behaviour of sandstone in CO₂ storage in aquifers. *Rock Mech Rock Eng* 49(2):417–426
- Zuo JP, Xie HP, Liu YJ, Hu B, Lu JF (2010) Investigation on fracture characteristics of sandstone after thermal effects through three-bending. *Acta Mech Solida Sin* 31(2):119–126 (**in Chinese**)